PUBLISHED VERSION (DOI): 10.1016/j.conbuildmat.2017.10.084

INTEGRATING GEOMATIC APPROACHES, OPERATIONAL MODAL ANALYSIS, ADVANCED NUMERICAL AND UPDATING METHODS TO EVALUATE THE CURRENT SAFETY CONDITIONS OF THE HISTORICAL BOCO BRIDGE

Álvaro Bautista-De Castro[1], Luis Javier Sánchez-Aparicio[1]*, Luís F. Ramos[2], José Sena-Cruz[2], Diego González-Aguilera[1]

[1]*Department of Cartographic and Land Engineering. University of Salamanca, High Polytechnic School of Ávila, Hornos Caleros, 50, 05003, Ávila (Spain)*

Tlf: +34 920353500; Fax: +34 920353501; alvarobautistadecastro@usal.es, luisj@usal.es, daguilera@usal.es

[2] *ISISE, Department of Civil Engineering, University of Minho, Campus de Azurém, 4800-058 Guimarães, Portugal; lramos@civil.uminho.pt, jsena@civil.uminho.pt*

**Corresponding author: Tlf.: +34 920353500; Fax: +34 920353501*

E-mail address: luisj@usal.es

Abstract

This paper proposes a multidisciplinary approach, combining the terrestrial laser scanner, ambient vibration tests and minor destructive tests, to characterize an early reinforced concrete bridge in Portugal: the Bôco Bridge. All methods are complemented by advanced numerical simulations and a coarse to fine calibration strategy, based on the Douglas-Reid and the non linear least squares approaches. Results obtained corroborate the robustness of the proposed approach, with an average relative error in frequencies of 1.2% and an average modal assurance criterion of 0.91. Considering this model, its current safety conditions were evaluated, obtaining a minimum safety factor of 2.1.

Keywords: historical bridge; reinforcement concrete; structural damage; terrestrial laser scanner; ambient vibration tests; finite element model updating.

1 Introduction

PUBLISHED VERSION (DOI): 10.1016/j.conbuildmat.2017.10.084

Transportation networks are fundamental elements in the economic development of countries, facilitating the communication and trade between different places (e.g. cities or villages). Inside the wide diversity of infrastructures that compose these networks, bridges are necessary elements to overpass topographic accidents, such as rivers or gullies. Considering them, as one of the most common, expensive and vulnerable infrastructures [1].

Among the variety of materials used in the construction of bridges, from masonry to steel [2], reinforced concrete (RC) has been one of the most used construction materials, especially after the development and popularization of the Hennebique [3] and Monier [4] systems in the beginnings of the XXth century. This popularity has been mainly due to its high availability, good mechanical properties (caused by the synergy between steel and concrete), moldability and low maintenance costs among other factors [5]. However, the aggressive environments on which the concrete bridges are constructed (usually with presence of chlorides, melting salts and carbon dioxide), tend to degrade this synergy. Degradation mainly governed by the destruction of the passivation layer (protection layer created between the concrete and steel bars promoted by the alkaline environment created into the concrete) due to the presence of chloride from melting salts and carbonation from atmospheric CO_2 among other factors. Promoting the penetration of the water and the oxygen and thus, the oxidation and volumetric expansion of the steel bars. Cracking the concrete elements and reducing the mechanical adhesion between components [6]. As a result, the bearing capacity of these infrastructures and their useful life can be considerably reduced.

Under the previous circumstances, the need to carry out studies to evaluate the current safety conditions of existing infrastructures, facing new demands of traffic loads, seems to be useful and necessary [7]. However, these evaluations are far from being trivial given the complexity of the geometry of early RC constructions (e.g. bars distribution), the inevitable presence of damages, the interaction between its structural elements and the supports, and the mechanical properties of the used materials. Placing the finite element method (FEM) as the most feasible solution to evaluate and simulate these structures [8-10]. However, and behind the advantages offered by this approach, able to evaluate a variety of structures submitted to different casuistic [11, 12], the

incorrect modelling of its geometry, boundary conditions, and mechanical properties may lead to erroneous results [13].

Under these premises, the present paper proposes a multidisciplinary method, based on the combination of terrestrial laser scanning procedures, ambient vibration tests, laboratory tests, advance numerical simulations, by means of FEM, and robust calibration strategies with the aim of creating accurate numerical simulations. Simulations able to reproduce accurately the current safety conditions of these structures. Particularly, this methodology has been validated in the historical RC bridge constructed over the Cávado river: the Bôco Bridge located in Braga, Portugal. This infrastructure was built in its origin according to the guidelines imposed by the Hennebique system in the year 1909 and later expanded, in order to withstand heavy traffic, in the year 1962. The low quality of the used concrete during this intervention has caused the degradation of its structural elements (mainly concrete spalling and steel corrosion). Being necessary the evaluation of its current carrying capacity under the actual loading demand.

Within this context, the paper is organized as follows: after is initial Introduction, Section 2 briefly describes the study case, its historical background, constructive system and current state of conservation; Section 3 shows the experimental campaign carried out on the bridge; Section 4 presents the calibration of the numerical model; Section 5 details the safety analysis carried out; and finally, in Section 6 the conclusions are drawn.

2 The Bôco Bridge

2.1 Historical background

Located along the road EM595-1, connecting the regions of Amares and Vieira do Minho, the Bôco Bridge is the actual oldest RC bridge in use in Portugal. Erected between the years 1909 and 1910 by the company Moreira de Sá & Malevez, following the project designed by the architect Sebasião Lopes (Fig. 1a). In the year 1950, the bridge was studied by engineers of different institutions reporting its bad state of conservation. The main damages found were concrete spalling and corrosion of the reinforcements, specially on the arches and deck.

Futhermore, the traffic was limited to a load of 5 tons per vehicle without crossing in the bridge at the same time until it was reinforced. In September 1961, the rehabilitation works started, following the project designed by the enginer J. Duarte Carrilho. Project that was ended in 1962 increasing the concrete sections and the reinforcenment of different structural elements [7] (Table 1).

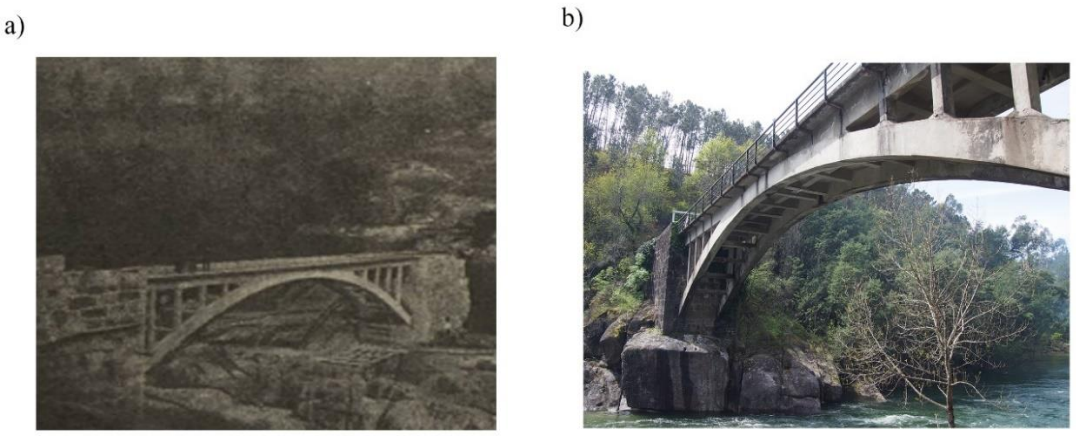

Figure 1: General views of the RC bridge evaluated: a) Bôco bridge in the year 1910 [7]; and b) current state of the Bôco bridge

Table 1: Original and current dimensions, reinforcement bars and stirrups of the different structural elements of the Bôco Bridge [7].

Structural element	Original dimensions (mm)	Original reinforcement bars (mm)	Original stirrups (mm)	Current dimensions (mm)	Added reinforcement bars (inches)	Added stirrups (inches)
Longitudinal arch girders (mid-span)	300 x 500	12 Ø 22	12	500 x 600	10 Ø 5/8 + 2 Ø 7/16	Ø 3/8
Longitudinal arch girders (at the abutments)	300 x 700	12 Ø 22	12	500 x 850	10 Ø 5/8 + 2 Ø 7/16	Ø 3/8
Pillars	250 x 250	4 Ø 15	12	350 x 320	4 Ø 1/2	Ø 5/16
Transverse girders	200 x 350	4 Ø 15	12	300 x 550	4 Ø 1	Ø 3/8
Central girder	200 x 300	4 Ø 15	12	300 x 350	2 Ø 3/4	Ø 7/16
Lateral longitudinal girders	200 x 500	4 Ø 15	12	300 x 550	-	-

2.2 Description of the bridge

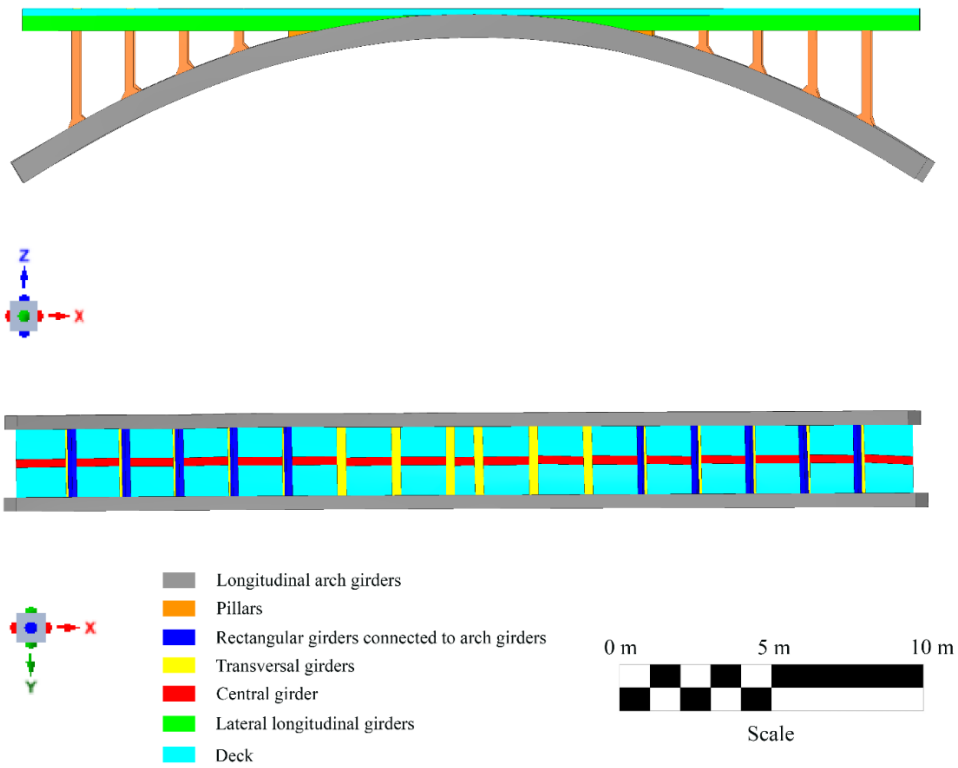

Figure 2: Structural elements of the Bôco Bridge.

The bridge is composed by 7 different structural elements (Fig. 2): i) two arch girders with an average cross-section of 500 × 725 mm (variable from their ends to the mid-span) and 35 m length, embedded its extrems in mansory walls; ii) 16 pillars spaced from each other 2 m with a cross-section of 350 × 320 mm, passing the loads from the lateral longitudinal girders to the arch girders; iii) 10 rectangular girders of 2.5 m length between the arch girders, making the bridge more rigid in the transversal direction; iv) 16 transverse girders with 2.7 m length that are connected to the lateral longitudinal girders and the central girder, with a cross-section of 300 × 550 mm, performing the same role that the rectangular girders connected to the arch girders; v) one central girder with 33 m length and a cross-section of 300 × 350 mm, with the ends supported on the masonry wall; vi) two lateral and longitudinal girders of 33 m length with a cross-section of 300 × 550 mm, supported on the masonry wall; vii) a deck, composed by a concrete shell with

120 mm of thickness; and viii) a overlay of granite with 130 mm of thickness placed on the concrete deck.

As stated in Section 2.1, the current structural elements of the Bôco Bridge have been the result of two stages, showing each one two concrete layers, namely (Fig. 3): i) old concrete, from the original desing; and ii) new concrete, added during the rehabilitations works.

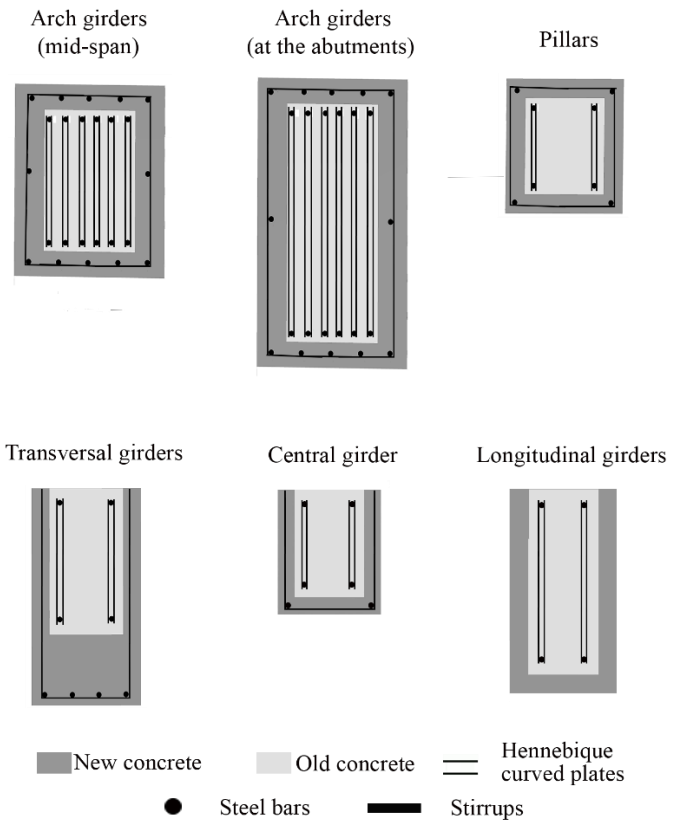

Figure 3: Cross-sections with concrete layers and reinforcement (steel bars, stirrups and Hennenbique curved plates) of the structural components. Adopted from [7].

2.3 Visual inspection

Results derived from the visual inspection carried out in 2016 corroborated the presence of different visual indicators of alteration, namely (Fig.4): i) concrete spalling; ii) salt crusts; iii) presence of moisture; iv) corrosion of the steel bars; v) cracks on the masonry supports; vi) algae; and vii) plants. Part of these damages, more specifically the concrete spalling and steel bars

corrosions, can be attributed to the high porosity (9.8 % in contrast with the 3.2 % of the old concrete layer) and the carbonation of the new concrete layer [7].

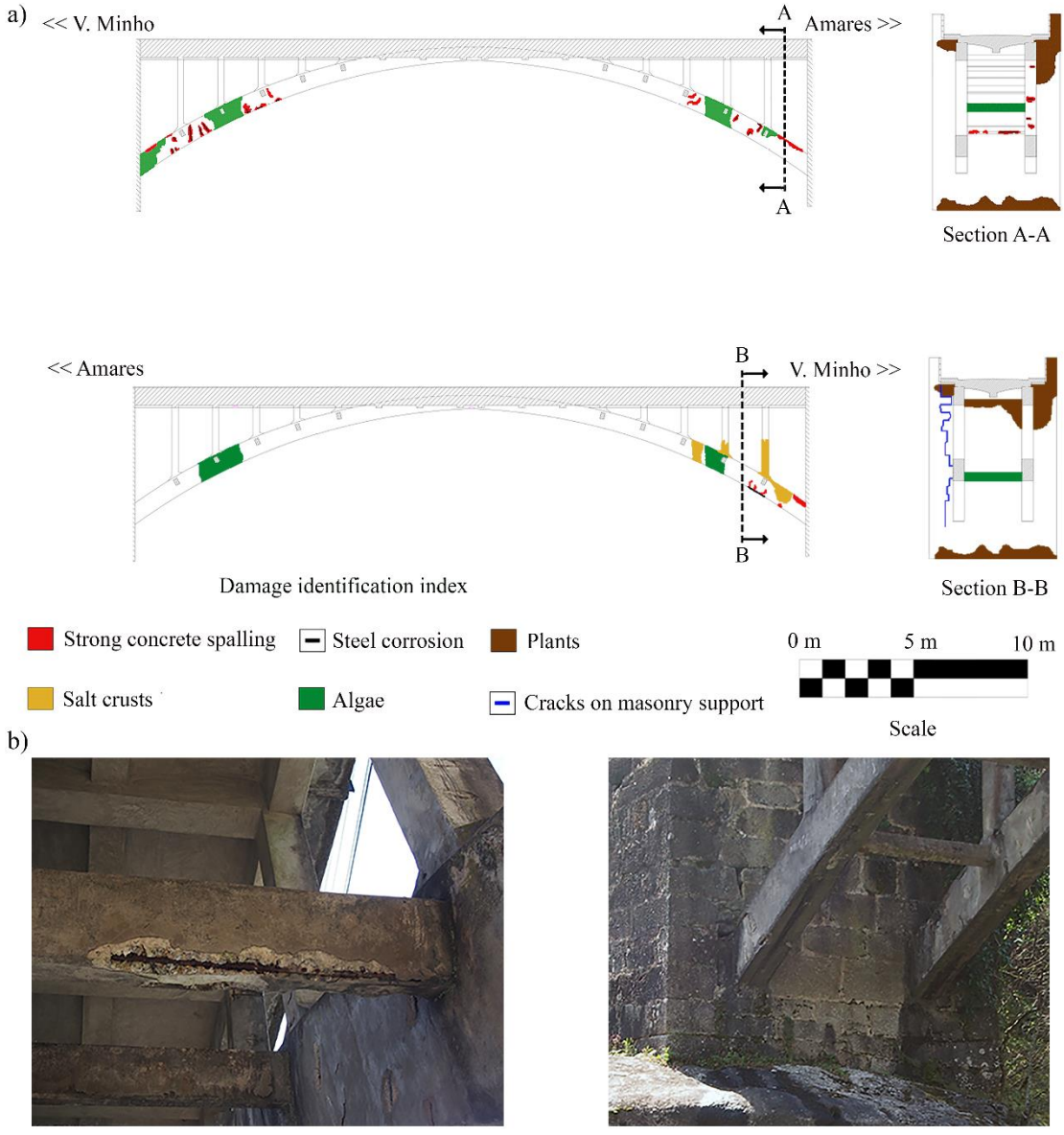

Figure 4: Results obtained from the visual inspection carried out: a) damage mapping; and b) current state of conservation.

3 Experimental program: geometrical, dynamic and material characterization of the bridge

3.1 Geometrical characterization: terrestrial laser scanner

Considering the complexity of the structure, as well as the lack of accessibility to certain zones, the lightweight Faro Focus 3D 120 TLS system (Table 2) (Fig. 5), based on the phase shift

physical principle [14], was used to assess the geometry of the bridge. Additionally to the TLS system, several registration spheres, with 20.0 cm and 14.5 cm of diameter (Fig. 5a), were used to align the different scans stations following the algorithm defined by [15].

Table 2: Technical specifications of the TLS Faro Focus 3D 120.

Faro Focus 3D 120	
Measurement principle	Phase shift
Measurement range	0.6-120 m
Accuracy nominal value	2 mm to 25 m in normal conditions of illumination and reflectivity
Field of view	360º Horizontal 305º Vertical
Capture rate	122,000/976,000 points
Beam divergence	0.19 mrad

Figure 5: TLS and registration spheres used during the data adquisition: a) during the recording of the deck; and b) TLS surveying at the lower part of the bridge.

As a result, 18 scan stations were needed to record the whole structure: i) 12 scans under the bridge; and ii) 6 scans on the bridge´s deck, obtaining an alignment error of 0.003 ± 0.002 m. The huge amount of data captured, with a total of 672,316,191 points, required an optimization of the point cloud for further evaluations. Applying to this end, the following decimation filters: i) a

distance filter with an average threshold of 40.0 m; and ii) a curvature-based decimation filter [16], with a threshold of 0.01 m, with the aim of simplifying flat areas while maintains relevant details, such as beam edges. As a result, an optimized 3D representation of the bridge was obtained, made up by 9,853,819 points (1.47 % of the original point cloud) (Fig. 6).

Figure 6: 3D representation of the bridge resulting of the point cloud optimization.

3.1.1 *From the point cloud to the as-built CAD model*

Common practices in the dynamic identification and numerical evaluation of bridges assume the *x* and *y* axis as the longitudinal and transversal axis of the structure [7, 10]. Being necessary the use of an additional procedure to place the bridge´s point cloud in the correct coordinate system (*x* axis representing the longitudinal axis of the bridge and the *y* axis the transverse one) (Fig. 7). To this end, the following workflow was used: i) the evaluation of the covariance matrix of the point cloud; ii) the analysis of the Eigen-values and Eigen-vectors of the covariance matrix; and iii) the rotation of the point cloud considering the angle between *x* axis and third eigenvector (direction of maximum dispersion of the bridge).

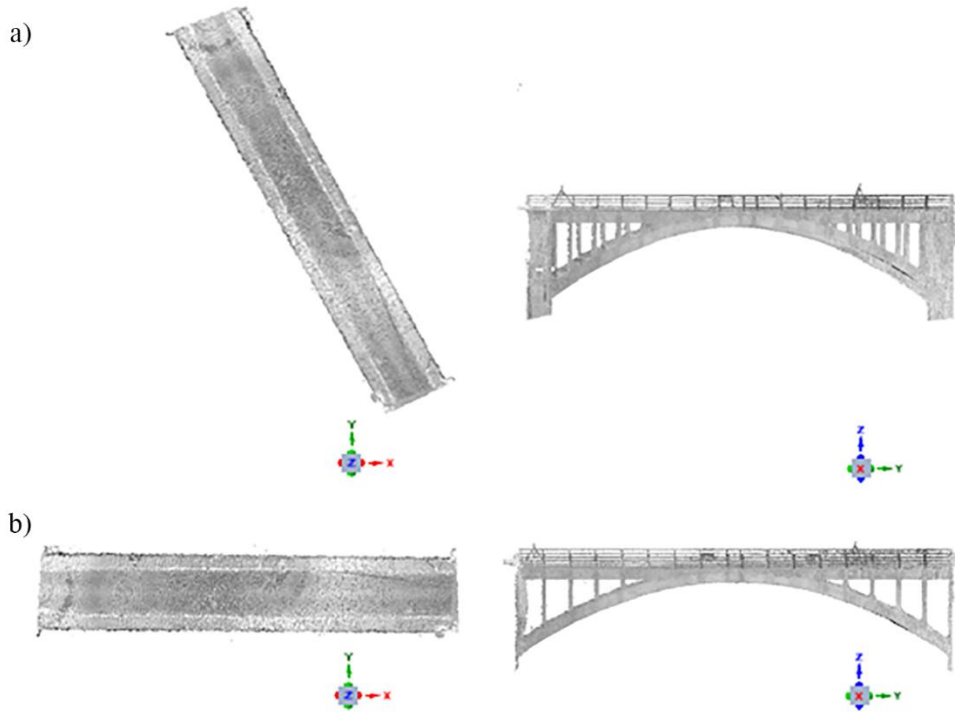

Figure 7: Results derived from the methodology proposed: a) original point cloud; and b) rotated point cloud**.**

With the aim of creating an accurate CAD model suitable for subsequent numerical evaluations, the geometrical modelling strategy used by [17] was considered, following the next stages: i) meshing the point cloud; ii) creation of the manifold mesh; and iii) creation of the CAD model, based on standard reverse engineering approaches [18]. As a result, an as-built CAD model was obtained (Fig. 8), on which the geometrical deviations during the bridge construction were taken into account (Fig. 9).

Figure 8: As-built CAD model obtained by the proposed method: a) plant view (arches A and B); and b) elevation view.

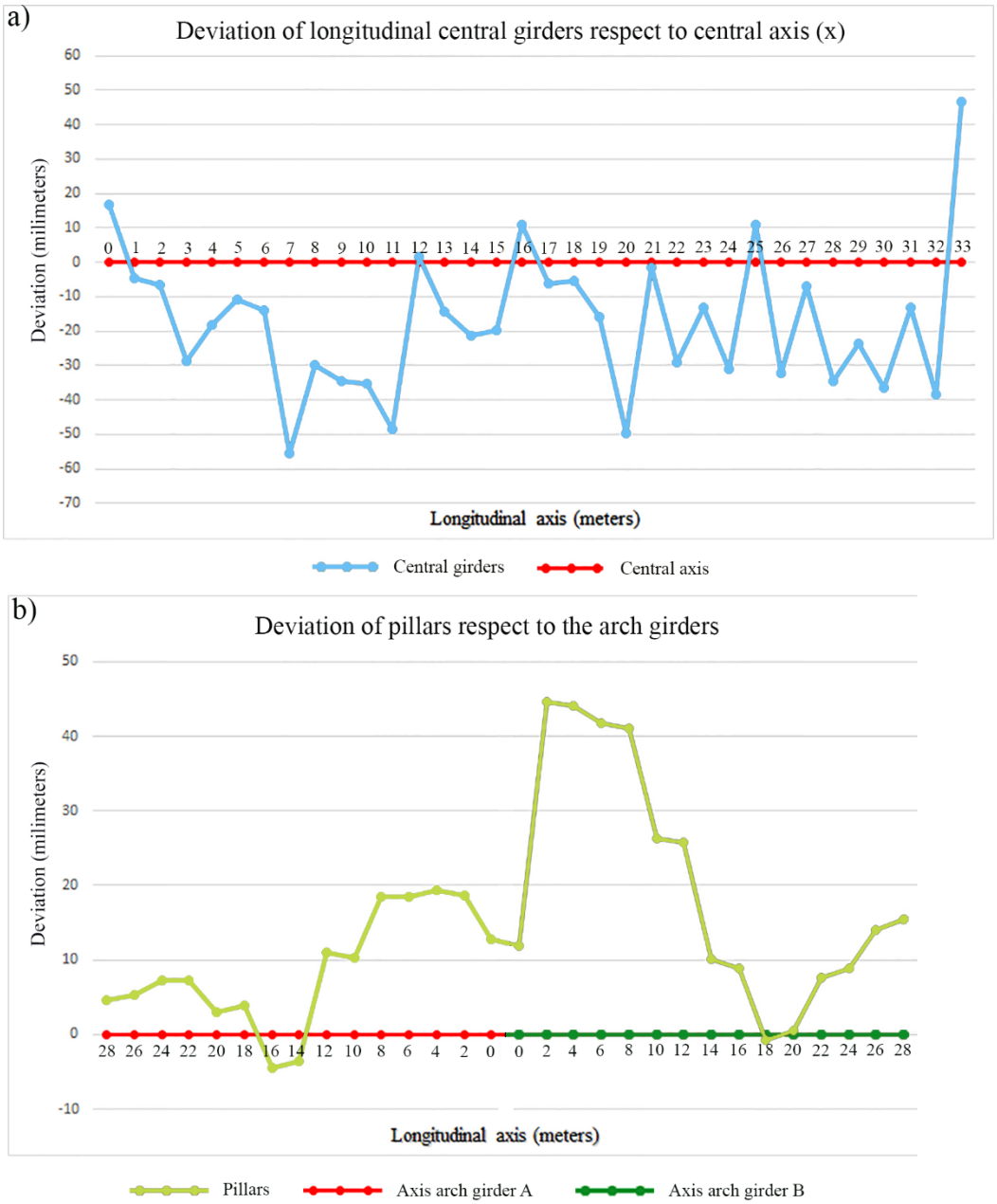

Figure 9: Deviations of structural elements with respect to their theoretical positions: a) longitudinal central girders; and b) pillars.

3.2 Ambient vibration tests

A dynamical identification campaign, based on the Operational Modal Analysis (OMA) approach, was performed with the purpose of identifying the modal properties of the bridge (such as the frequencies, damping ratios and modal shapes). To this end, two setups with an acquisition time of 20 min and a sampling rate of 256 Hz, were used. In each one, a total of 14 uniaxial piezoelectric accelerometers, with a sensitivity of 10 V/g, range of ±0.5g and 8μg rms broadband resolution, were placed along the bridge´s deck. Considering 5 accelerometers as references

(Fig.10): i) accelerometers (3), (11), and (6) in the Z direction; and ii) accelerometers (4) and (6) in the Y direction.

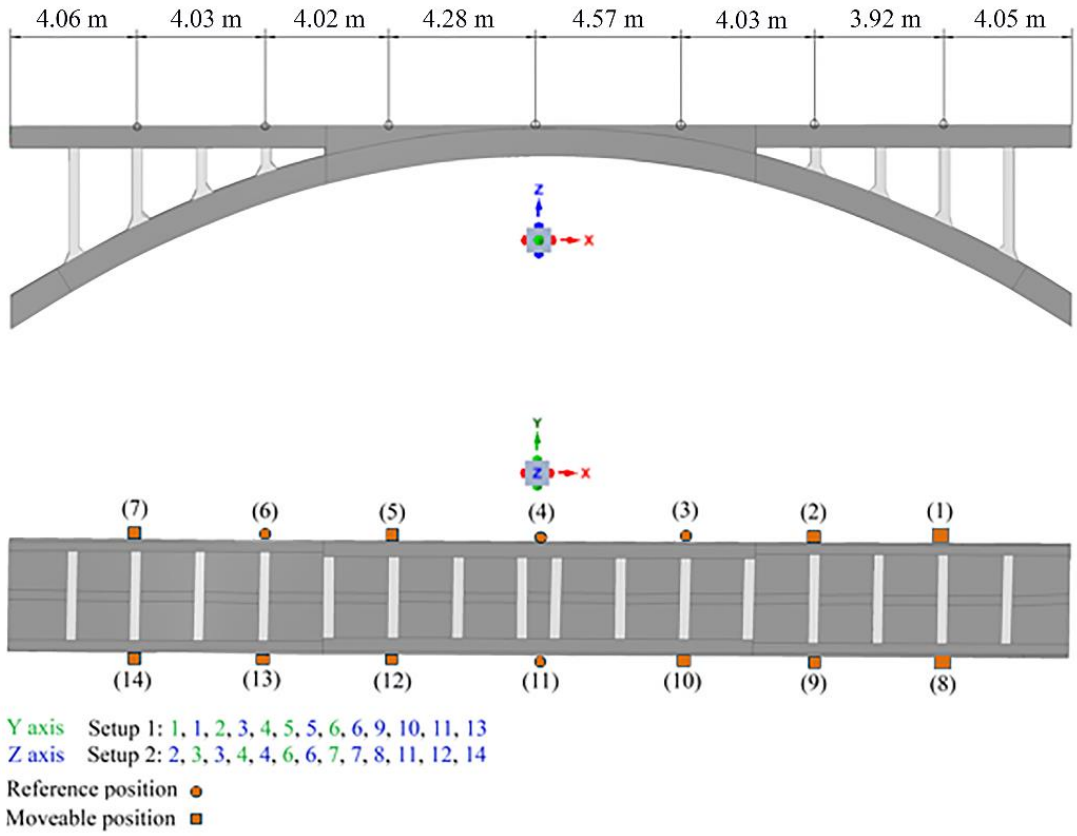

Figure 10: Accelerometers positions and setups used during the ambient vibration tests.

Finally, to extract the dynamic properties the Enhanced Frequency Domain Decomposition algorithm (EFDD), based on the power spectral density, was used to extract the modes [19]. As a result, 12 modes were identified with a range of frequencies between 4.15 Hz to 27.13 Hz (Table 3) (Fig. 11). The low coefficient of variation (CoV) for frequencies and damping ratios show the quality of the identified modal properties. On average, the damping ratio was equal to 1.67%.

PUBLISHED VERSION (DOI): 10.1016/j.conbuildmat.2017.10.084

Table 3: Natural frequencies and damping ratios obtained.

Mode shape	Frequencies (Hz)	CoV (%)	Damping ratios (%)	CoV (%)	Description
1	4.15	0.02	1.91	1.70	1st translational
2	6.51	<0.01	2.13	2.60	1st vertical bending
3	9.88	0.01	0.62	1.75	2nd vertical bending
4	11.53	0.02	1.54	2.57	3rd vertical bending
5	11.75	0.02	1.36	2.99	1st torsional
6	12.34	0.01	2.47	2.41	2nd torsional
7	14.11	0.04	2.43	6.15	3rd torsional
8	18.71	0.03	3.95	3.13	4th vertical bending
9	19.95	0.01	1.29	1.18	4th torsional
10	21.67	0.01	2.11	1.27	5th torsional
11	26.56	0.02	4.69	0.59	5th vertical bending
12	27.13	0.01	1.70	0.98	6th torsional

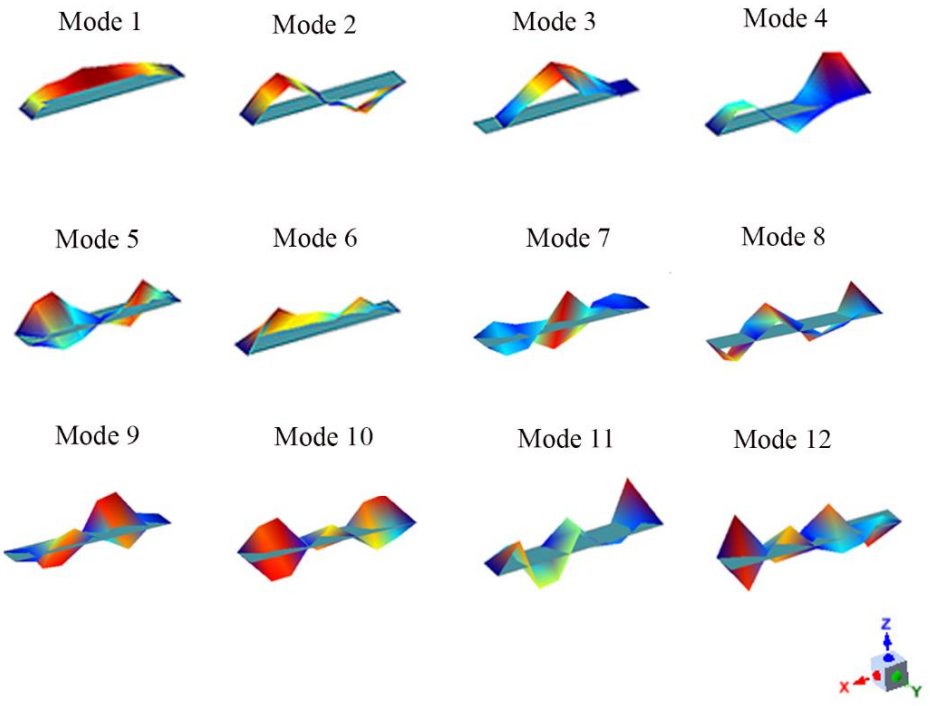

Figure 11: Graphical representation of the vibrational modes extracted by the EFDD algorithm.

PUBLISHED VERSION (DOI): 10.1016/j.conbuildmat.2017.10.084

3.3 Material characterization

Built in RC, the Bôco Bridge shows in each structural component a total of 2 layers namely: i) old concrete and ii) new concrete layer. According with this disposition, several mechanical and chemical tests were carried out in a previous experimental campaign to characterize the concrete and the steel of the bridge [7], extracting samples from different locations as shown Figure 12.

Results derived from the mechanical (through compression tests, chemical tests and gravimetric procedures) and physical characterization of the concrete used in the Bôco Bridge, corroborated the low quality of the new concrete layer. Showing a material with low compression resistance (Table 4) as well as a high porosity (around 9.8% with a coefficient of variation of 8.6%). This physical property, the porosity, have caused the presence of carbonatation effects on the new layer [7] and thus, steel corrosion and consequently concrete spalling along the different structural components of the bridge (Fig. 4b).

Table 4: Results obtained from the compression tests carried out by [7]. Young Modulus (*Ec*) of the new concrete have been estimated through the relation proposed by [20].

	Old concrete		**New concrete**	
Structural element	*Ec* (GPa)	$f_{is,cyl}$ (MPa)	*Ec* (GPa)	$f_{is,cyl}$ (MPa)
Arch (C1)	-	-	24.80	14.9
Deck (C10)	-	-	29.70	27.2
Pillar (C3)	54.08	58.8	-	-
Pillar (C4)	45.73	48	-	-
Pillar (C5)	-	59.2	-	-
Arch (C6.2)	43.15	58	-	-
Deck (C9)	36.61	29.9	-	-
Deck (C11)	-	64.8	-	-
Deck (C12.2)	26.86	46.1	-	-

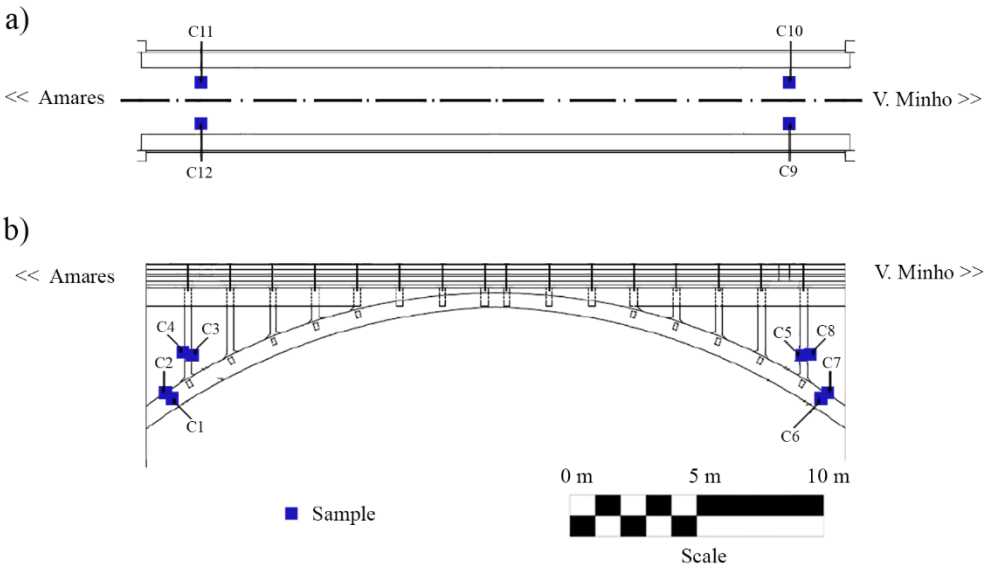

Figure 12: Locations of the samples taken from the bridge by [7]: a) top view; and b) elevation view

Regarding the steel used in the reinforcement bars, four samples were extracted and characterizing in laboratory using the following tests: (i) scanning electron microscope with X-ray fluorescent spectrometer; and (ii) carbon element tests. As a result, was possible to conclude that the steel used in the bridge was mild steel (presenting inclusions of manganese sulphide) [7].

4 Modelling the current state of the Bôco Bridge

Negative effects that bridges present, without a proper maintenance plan, can increase when time elapses, reducing its load capacity [21]. It is for this reason that is necessary not only to carry out extensive experimental campaigns, focused on the characterization of the different structural components, damages or mechanical properties, but also numerical simulations to evaluate the current safety conditions of the bridge. These models need to be contrasted with experimental data, such as ambient vibration tests, to validate them.

4.1 Construction of the numerical model

According with the exposed above, a numerical simulation by means of FEM was carried out. To this end, the software TNO Diana ® [22] was used together with a numerical mesh composed of 193,814 elements (Fig. 13): i) 193,546 solid elements for the structural components and ii) 268 interface elements for the simulation of the interaction of the structure with its supports.

PUBLISHED VERSION (DOI): 10.1016/j.conbuildmat.2017.10.084

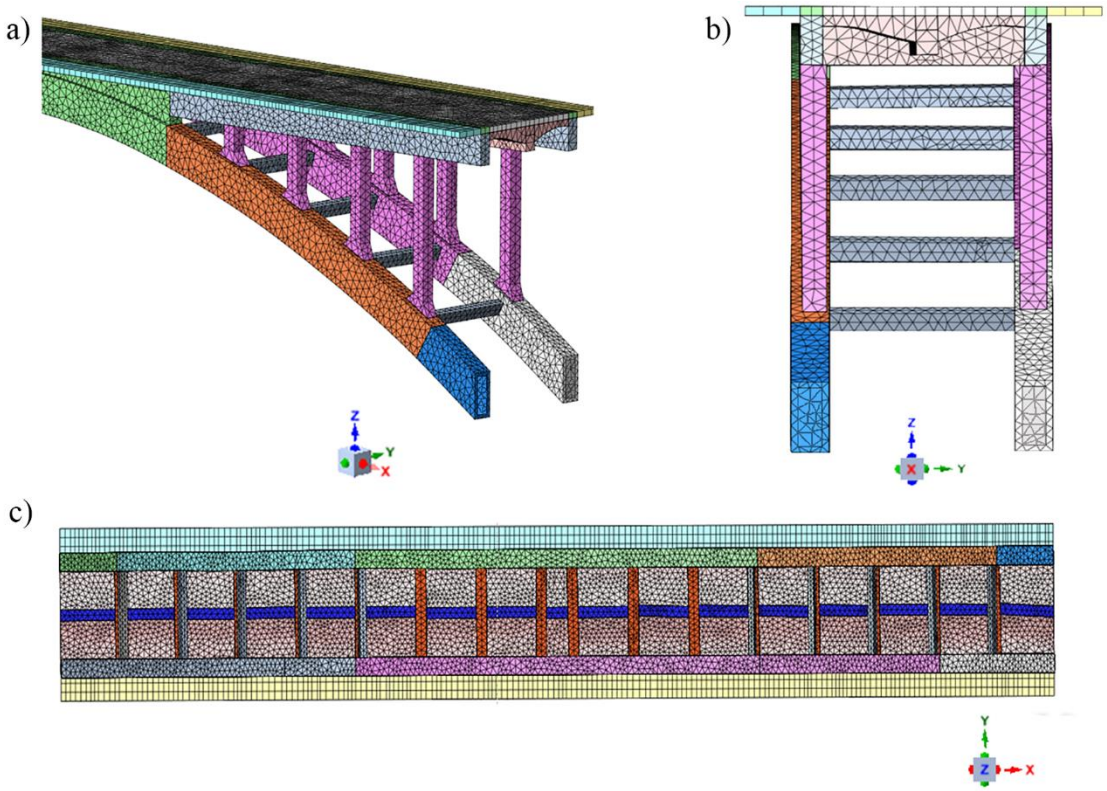

Figure 13: Mesh of numerical model utilized: a) isometric view; b) front view and c) plant view.

As it was described in Section 2, the different structural components of the bridge were retrofitted, showing each element two layers composed by concretes with different mechanical properties (Table 4). With the aim of reducing the complexity of the numerical simulation and thus, the computational effort, a homogenous concrete section was considered on each structural element. Therefore, the numerical model was divided in 5 groups according with the similarity, in terms of concrete properties, between structural components (Fig. 3) (Fig. 14).

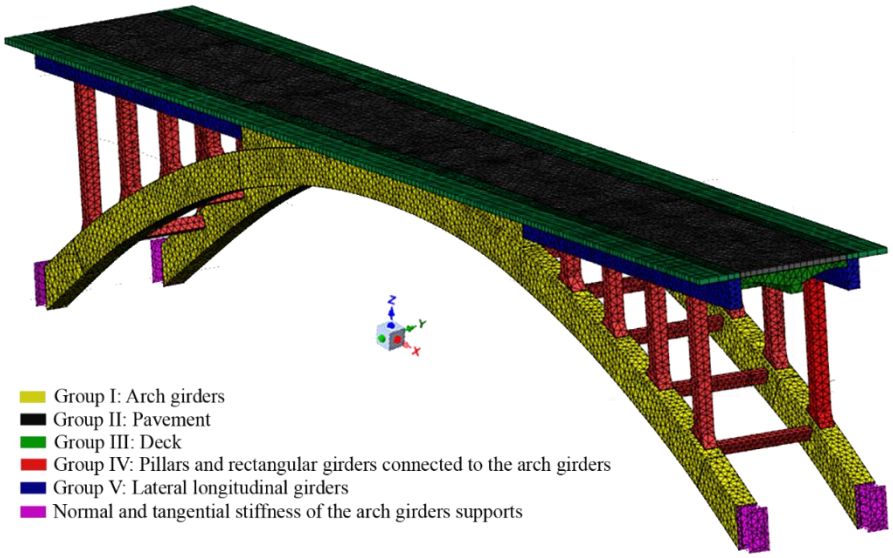

Figure 14: Elements' groups considered during the calibration stage.

To pass from the heterogeneous section (sections with the two concrete layers) to the equivalent homogeneous section, the following variables were calculated: i) equivalent density; and ii) equivalent Young Modulus.

On one hand, the equivalent density of each group was calculated through the weighted arithmetic mean (considering as weight the percentage in volume of the two concrete in the structural element evaluated) (Fig. 3), taking into account as base values those obtained in the previous experimental campaign [7] (Table 5). On the other hand, the equivalent Young Modulus of each group was obtained according with the following workflow (Fig. 15). Using the relation exposed in (Eq. 1) [23] to obtain the equivalent Young Modulus and the mechanical properties obtained in the previous experimental campaign [7] (Table 5).

Table 5: Average, upper and lower Young Modulus and density values considered during the homogenization stag.

	Young Modulus (GPa)		Density (kg/m^3)	
	Old concrete	New concrete	Old concrete	New concrete
Upper bound	62	34	2607	2217
Average	41	27	2418	2144
Lower bound	21	20	2229	2071

$$E_{updated} = \mathrm{E}_{initial} \times \left(\frac{f_{i,j}^{ref}}{\mathrm{f}_{i,j}^{num}} \right)^2 \quad (1)$$

where $E_{updated}$ is the calibrated equivalent Young Modulus; $E_{initial}$ is the initial value of the equivalent Young Modulus (homogenous section); $f_{i,j}^{ref}$ is the reference frequency (homogeneous section) obtained from the eigenvalue analysis of the group *i* (heterogeneous section) for the mode *j*; and $f_{i,j}^{num}$ is the frequency (homogeneous section) derived from the eigenvalue analysis of the group *i* for the mode *j*.

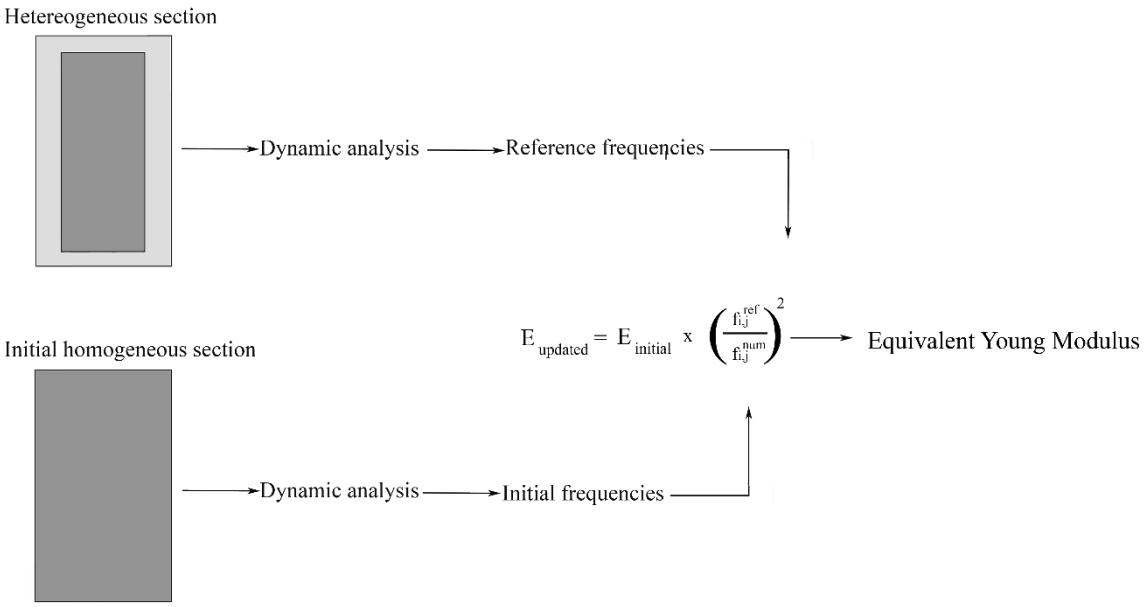

Figure 15: Proposed workflow to obtain the equivalent Young modulus.

As a result, the following equivalent values were obtained (Table 6) for the different groups considered.

Table 6: Average, upper and lower equivalent Young Modulus and equivalent density values obtained during the homogenization stage.

		Upper bound	Average	Lower bound
Group I	*E* (GPa)	45	33	21
	Density (Kg/m^3)	2412	2281	2150
Group III	*E* (GPa)	39	31	22
	Density (Kg/m^3)	2500	2307	2114
Group IV	*E* (GPa)	30	22	13
	Density (Kg/m^3)	2410	2297	2184
Group V	*E* (GPa)	33	24	15
	Density (Kg/m^3)	2434	2310	2186

Concerning the Group II, the pavement (granite blocks without mortar), the Young Modulus provided by [24], with a value of $E = 0.2 \pm 0.14$ GPa, was considered.

4.2 Initial results

Taking into account the average equivalent Young Modulus obtained in Table 6, as well as the boundary conditions used during the evaluation of the Luiz Bandeira bridge (erected in the same epoch and with the same construction system) [9], an initial evaluation was carried out.

To validate the accuracy of the numerical model, the relative error in frequencies and the modal assurance criterion (MAC) [25] were taken into account. Considering for these purpose, the first six frequencies and modal shapes (integrated by flexural and torsional modes). Results derived for this initial model shown a rigid structural system, especially in the transversal direction (modes 1,5,6) (Table 7), in comparison with the results obtained during the AVT.

Table 7: Comparison between experimental and numerical frequencies and MAC values from the initial model.

Vibration modes	f_{exp} (Hz)	f_{num} (Hz)	Relative error (%)	MAC
1	4.15	5.52	32.96	0.85
2	6.52	6.31	3.07	0.97
3	9.88	10.77	8.97	0.97
4	11.53	13.61	18.06	0.75
5	11.81	26.07	120.76	0.85
6	12.34	13.69	10.92	0.81

4.3 Finite element model updating strategy

As shown in the previous section, the first numerical simulation presented great discrepancies between the numerical and the experimental data, with an average relative error in frequencies of 32.46% and an average MAC value of 0.87, thus a calibration process able to minimize the discrepancies between the numerical and experimental modal responses was required.

From a mathematical point of view, the calibration of a numerical model can be considered as a constrained optimization problem [26], being possible to use two types of calibration methods: i) global optimization approaches or ii) local optimization algorithms. On one hand, the global optimization strategies can be used to find the global minimum of the cost function (function to be minimized), involving a high number of evaluations and thus large computational times, especially when the numerical model is complex [10]. On the other hand, local approaches can be used to find the nearest minimum of the cost function (which generally is a local minimum), using to this end a low number of evaluations, being more practical for complex simulations [13]. According with these premises, in this paper a coarse to fine calibration strategy is proposed of the following sequential stages: i) a global sensitivity analysis based on the Spearman correlation method [27] and the Latin hypercube sampling strategy [28] in order to evaluate the more sensible parameters; ii) a coarse calibration by means of the Douglas-Reid (DR) method [29] and the

genetic algorithm [30]; and iii) a fine calibration through the non-linear least-squares strategy. Equation 2 define the cost function used during the calibration stage.

$$J = \frac{1}{2}\left[W_f \sum_{i=1}^{m}\left(\frac{f_i^{num} - f_i^{exp}}{f_i^{exp}}\right)^2 + W_{MAC}\sum_{i=1}^{m}(1 - MAC_i)^2\right] \quad (2)$$

where f_i^{num} and f_i^{exp} are the numerical and experimental frequencies for mode *i* respectively, MAC the modal assurance criterion of the mode *i*, W_f the frequency weight and W_{MAC} the MAC weight.

Considering the cost function defined in (Eq. 2), the DR algorithm was used to estimate the surface response (Eq. 3), requiring a total of 2*n* + 1 evaluations, being *n* the numerical variables to be calibrated.

$$R_i^{num} = \sum_{k=1}^{n}[A_{ik}X_k + B_{ik}X_k^2] + C_i \quad (3)$$

where R_i^{num} is the i^{th} frequency or MAC values; A_{ik}, B_{ik} and C_i are the coefficients of the second order function; and X_k the *k* numerical variable applied during the calibration. Complementary to the DR algorithm, , a genetic algoritm was applied to find the global minimum of the DR response surface. Finally, the global minimum of the DR response surface was refined through a the robust calibration method based on the non-linear least squares (LS), the gradient-based Gauss Newton and the trust region reflective algorithms as exposed [31].

4.3.1 *Numerical model 1: calibration A*

Considering the workflow proposed in the previous section, a global sensitivity analysis was carried out using 1500 samples (obtained through the Latin hypercube sampling method) and a total of 14 parameters, given by: i) five Young Modulus (*Eb1* to *Eb5*) and densities (*db1* to *db5*), representing the five groups previously defined (Fig. 14); ii) the normal and tangential stiffness of the deck supports (*Kn1* and *Kt1*); and iii) the normal and tangential stiffness of the arch girders supports (*Kn2* and *Kt2*).

On one hand, upper and lower bounds obtained in Table 6 were used as limits for the density and Young Modulus, respectively. On the other hand, and according with the literature [10, 13, 32, 33], $1x10^{10}$ N/m^3 and $1x10^{7}$ N/m^3 were used as suitable upper and lower bounds, respectively, for the interface elements considered.

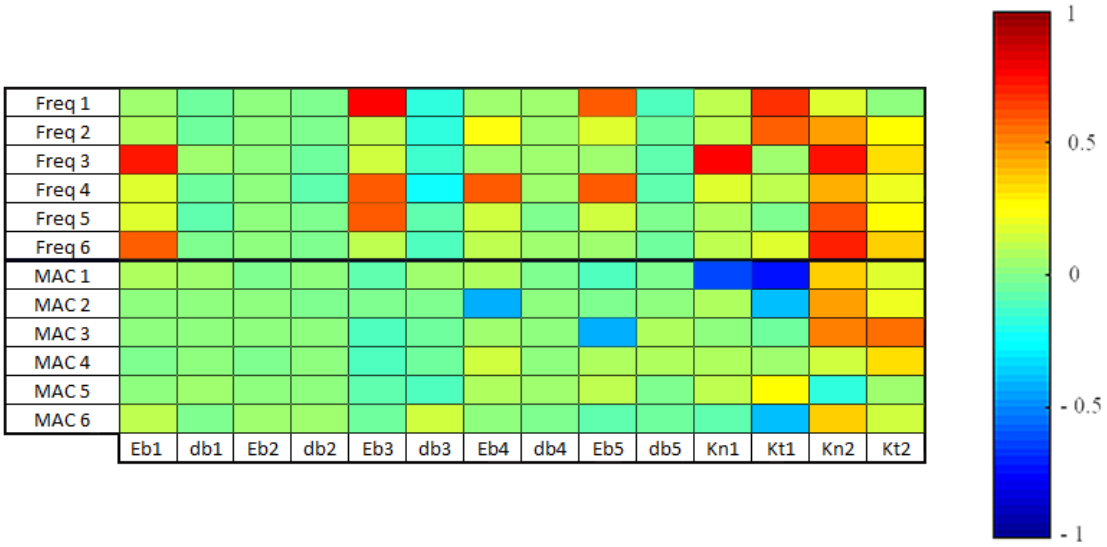

Figure 16: Linear Spearman correlation matrix obtained during the first calibration (A).

From the results obtained during the sensitivity analysis (Fig. 16), the following eight parameters were considered as suitable calibration variables: i) four Young Modulus, corresponding with the groups I, II, IV and V; and ii) the normal and tangential stiffness of the deck and arch girder supports.

As was exposed in Section 4.3, the DR method and the genetic algorithm (with 50 individuals, 150 generations and a cross-over fraction of 0.8) was used to estimate the rough minimum of the cost function. The initial population used in the genetic algorithm was randomly generated by the Latin hypercube sampling method. Finally, this minimum was refined with the LS method (Table 8 and Table 9).

Table 8: Updated values obtained during the DR and LS calibration.

Parameter	Upper bounds	Lower bounds	DR	LS
Eb1 (GPa)	47.95	20.59	31.08	29.96
Eb3 (GPa)	38.68	22.40	33.13	29.24
Eb4 (GPa)	29.63	22.79	29.52	28.66
Eb5 (GPa)	33.17	22.97	31.05	28.92
Kn1 (N/m^3)	1 x 10^{10}	1 x 10^7	1.91 x 10^7	1.36 x 10^7
Kt1 (N/m^3)	1 x 10^{10}	1 x 10^7	3.44 x 10^8	4.48 x 10^8
Kn2 (N/m^3)	1 x 10^{10}	1 x 10^7	6.14 x 10^9	6.35 x 10^9
Kt2 (N/m^3)	1 x 10^{10}	1 x 10^7	2.84 x 10^9	3.94 x 10^9

Table 9: Discrepancies obtained during the calibration A in terms of relative error in frequencies (*f*) and MAC values. In brackets, values achieved during the DR calibration.

Vibration modes	f_{exp} (Hz)	f_{num} (Hz)	Relative error (%)	MAC
1	4.15	4.19 (4.21)	1.02 (1.42)	0.93 (0.94)
2	6.51	6.42 (6.53)	1.37 (0.34)	0.97 (0.97)
3	9.88	9.53 (10.04)	3.55 (1.63)	0.97 (0.97)
4	11.53	11.71 (12.08)	1.56 (4.77)	0.83 (0.78)
5	11.81	11.57 (12.90)	2.05 (9.23)	0.88 (0.88)
6	12.34	12.64 (11.75)	2.42 (4.78)	0.82 (0.82)

The average values of the calibration A (Table 8) for the relative error frequencies and MAC were 1.99 % and 0.90, respectively. Comparing with the calibration performed by DR with the average values of the relative error frequencies and MAC, 3.70 % and 0.89 were obtained, respectively.

These results demonstrate that the LS method reduces the difference between numerical and experimental frequencies but doesn't significantly increases the MAC values.

To evaluate the possible origin of these discrepancies, the coordinate modal assurance criterion (COMAC) [25] was used. Results derived from this index show a concentration of discrepancies in the first, eighth, fifteenth and twenty-first degree of freedom (Fig. 17). These discrepancies correspond with the supports of the arch girders as well as the areas with higher concentration of damages (see Section 2.3 and Section 3.2).

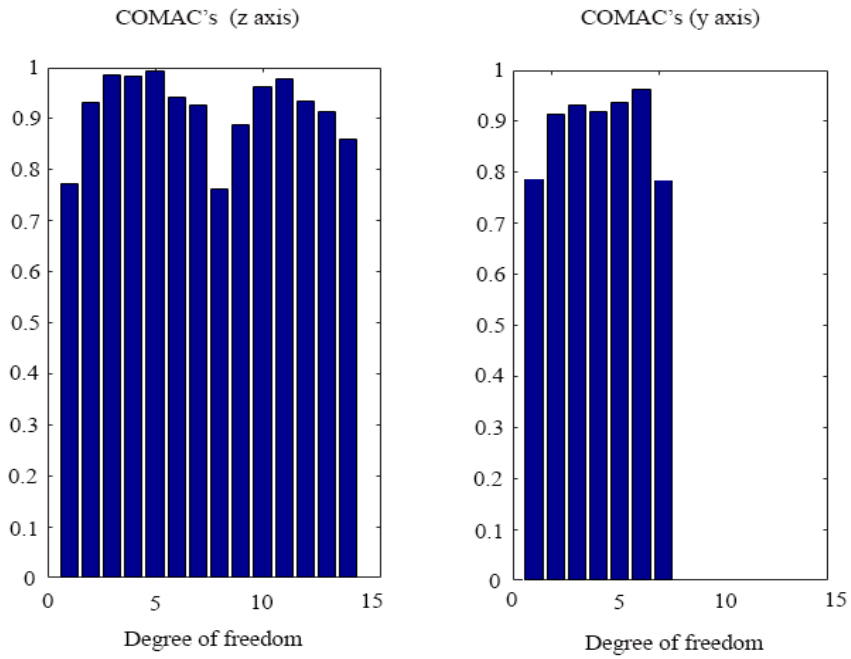

Figure 17: COMAC values obtained during the first calibration: a) COMAC values in *z* axis; and b) COMAC values in *y* axis.

4.3.2 *Numerical model 2: calibration B*

Although the results obtained during the calibration A can be considered with acceptable accuracy (Table 9) (Fig. 17), a second calibration stage, named calibration B, was carried out with the aim of minimizing its discrepancies and provided a more accurate numerical simulation.

Considering the results obtained during the AVT, with asymmetric modes (Fig. 11), as well as the high discrepancies observed in the first, eighth, fifteenth and twenty-first degrees of freedom (Fig. 17), additional parameters were introduced in the sensitivity analysis, namely (Fig. 18): i)

damages in the arch girders, *Db1*, *Db2*, *Db4* and *Db5*; ii) damage in a support of the arch girder B, *Db6* (Fig. 4b) (Fig.8) and iii) damages in a pillar, *Db3*.

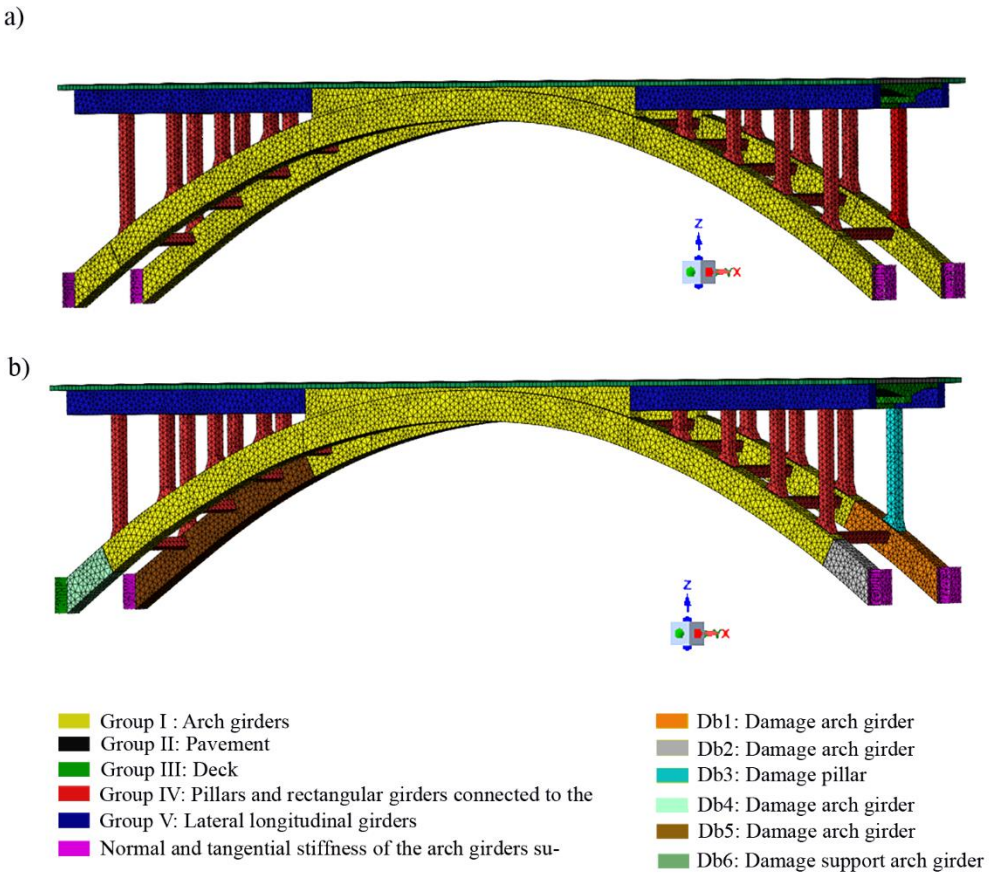

Figure 18: Comparison between numerical models: a) numerical model 1; and b) numerical model 2

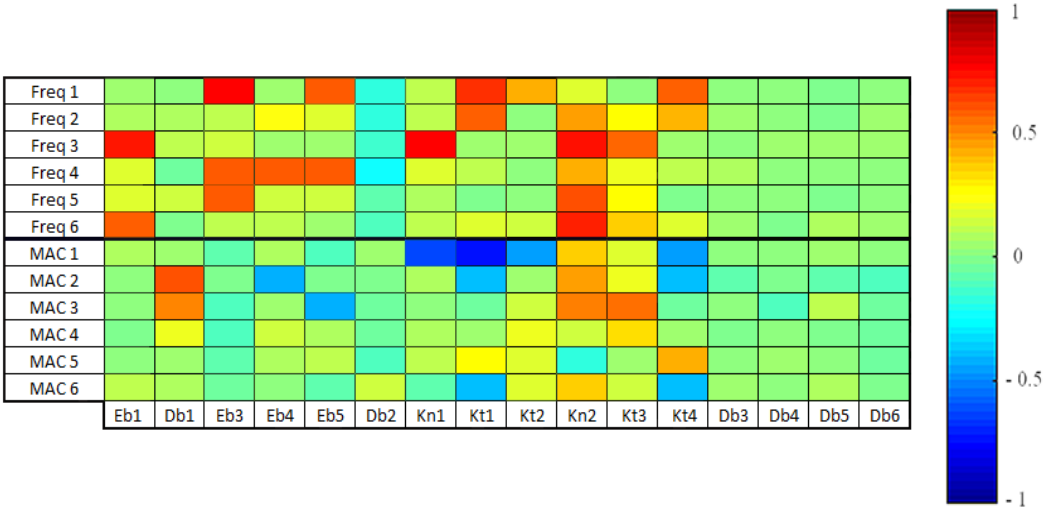

Figure 19: Linear Spearman correlation matrix obtained during the second calibration (B).

From the evaluation of the Spearman correlation matrix (Fig. 19) two additional considerations were taken into account to improve the numerical calibration: i) the parameter *Db1*; and ii) an orthotropic behaviour of the supports. Therefore, in this analysis 12 calibration variables were considered (Fig. 20): i) 9 from the calibration A; ii) one variable that represent the damage on the arch girder; and iii) two additional shear stiffness on the deck and on arch girders supports.

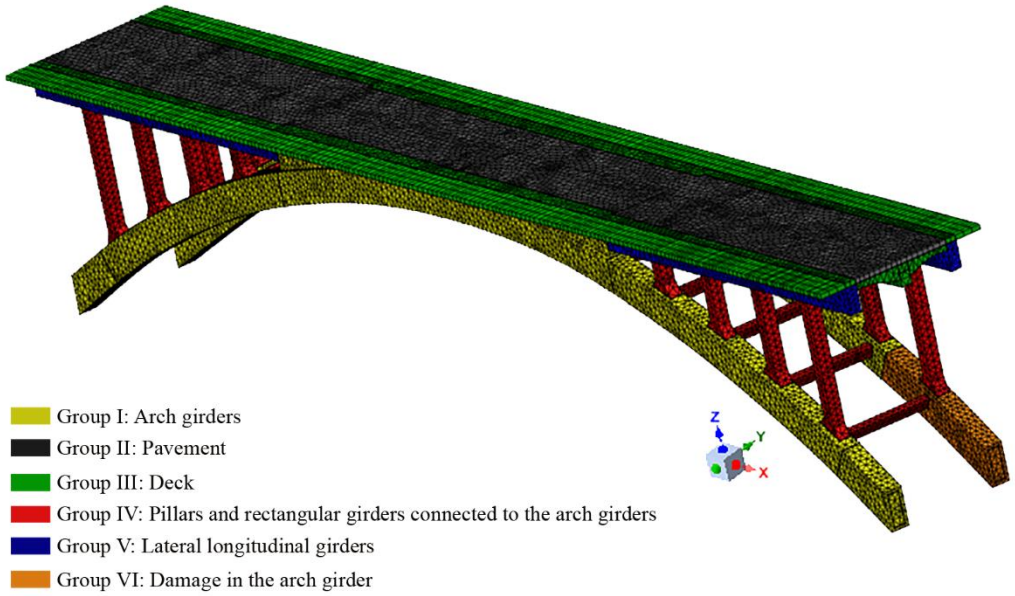

Figure 20: Concrete groups considered during the second calibration (B).

For this second calibration, only the robust calibration (LS method) was used. Using as starting values the results obtained during the calibration A. Thus, a more accurate simulation of the bridge, with an average relative error in frequencies of 1.22 % and an average MAC value of 0.91 (Table 10) (Fig.21), was obtained.

Table 10: Discrepancies between the experimental and numerical data obtained during the second calibration stage (B). In brackets, the discrepancies of the initial model.

Vibration modes	f_{exp} (Hz)	f_{num} (Hz)	Relative error (%)	MAC
1	4.15	4.17 (5.52)	0.53 (32.96)	0.93 (0.85)
2	6.51	6.53 (6.31)	0.24 (3.07)	0.97 (0.97)
3	9.88	9.61 (10.77)	2.68 (8.97)	0.96 (0.97)

4	11.53	11.60 (13.61)	0.64 (18.06)	0.87 (0.75)
5	11.81	11.92 (26.07)	0.97 (120.76)	0.90 (0.85)
6	12.34	12.62 (13.69)	2.25 (10.92)	0.84 (0.81)

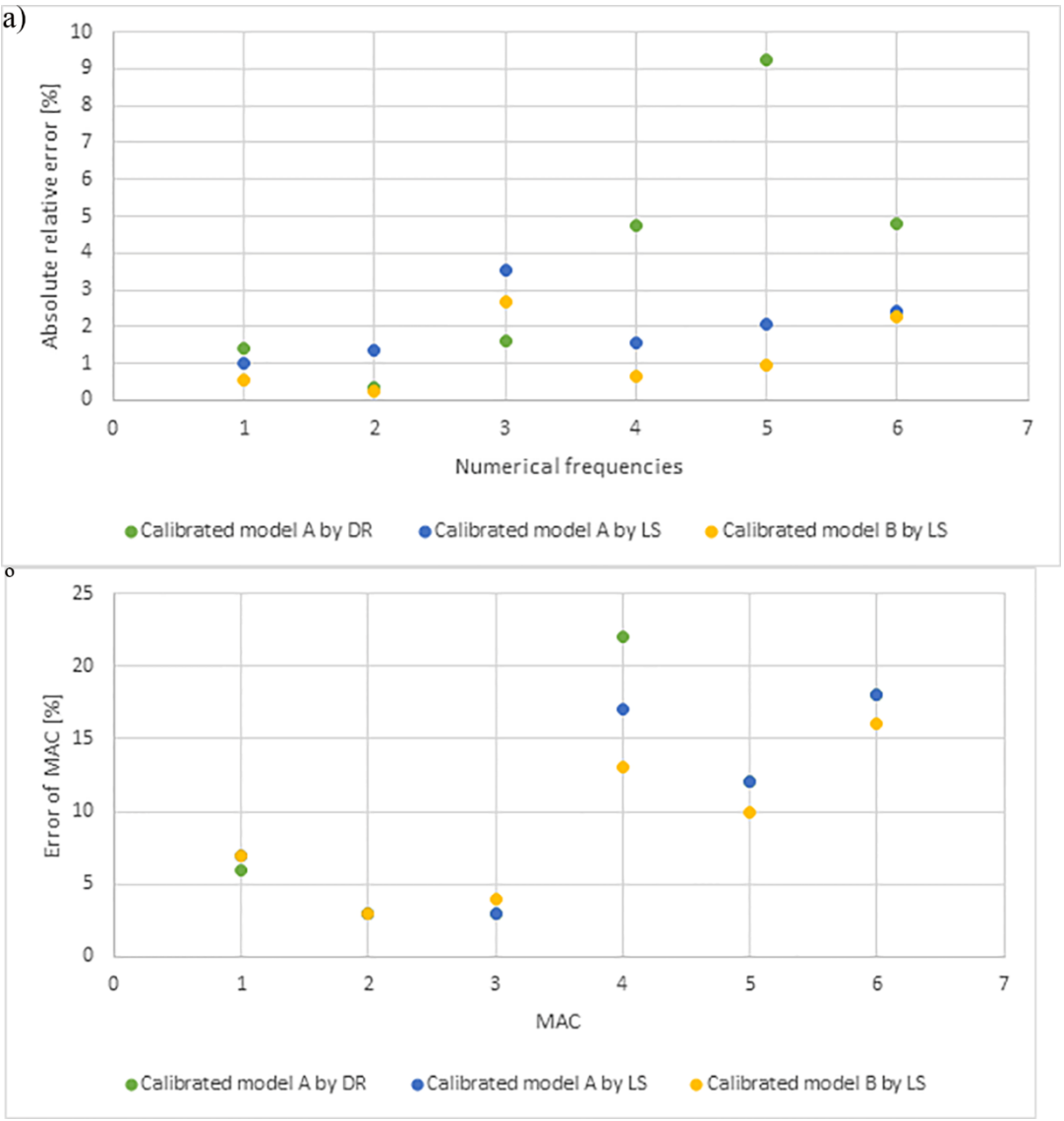

Figure 21: Errors obtained during the different calibrations (A, B): a) Absolute relative error in frequencies; b) Relative error in MAC values.

Table 11: Updated values obtained during the different calibration stages.

Parameter	Upper bounds	Lower bounds	Calibration A	Calibration B
Eb1 (GPa)	47.95	20.59	29.96	29.79
Db1 (GPa)	47.95	20.59	29.96	27.80
Eb3 (GPa)	38.68	22.40	29.24	30.07
Eb4 (GPa)	29.63	22.79	28.66	27.92
Eb5 (GPa)	33.17	22.97	28.92	28.60
Kn1 (N/m^3)	1×10^{10}	1×10^{7}	1.36×10^{7}	1.04×10^{7}
Kt1 (N/m^3)	1×10^{10}	1×10^{7}	4.48×10^{8}	5.60×10^{8}
Kt2 (N/m^3)	1×10^{10}	1×10^{7}	4.48×10^{8}	4.22×10^{8}
Kn2 (N/m^3)	1×10^{10}	1×10^{7}	6.35×10^{9}	6.24×10^{9}
Kt3 (N/m^3)	1×10^{10}	1×10^{7}	3.94×10^{9}	4.34×10^{9}
Kt4 (N/m^3)	1×10^{10}	1×10^{7}	3.94×10^{9}	3.95×10^{9}

Concerning the updated parameters achieved in the different calibrations carried out (Table 11), especially the Young's Modulus variables (average value of 28.84 GPa), it is possible to corroborate a generalized damage of the new concrete layer observed during the visual inspection carried out (see Section 2.3) showed similar results that those obtained in Section 4.1 (average value of 30.81 GPa). In what regards to the calibrated stiffness, low values were obtained on the deck in the normal direction (1.04×10^{7} N/m^3) with respect to the tangential stiffness (4.91×10^{8} N/m^3) where obtained and higher values for the interfaces that define the interaction between the arch girders and the abutments (average value of 4.84×10^{9} N/m^3).

Finally, Fig. 22 shows a graphical comparison between the experimental and numerical mode shapes. Analysing all results, one can conclude that the results derived from the second approach show a reasonable better correlation with the ones obtained from AVT (Fig. 21) (Fig. 22).

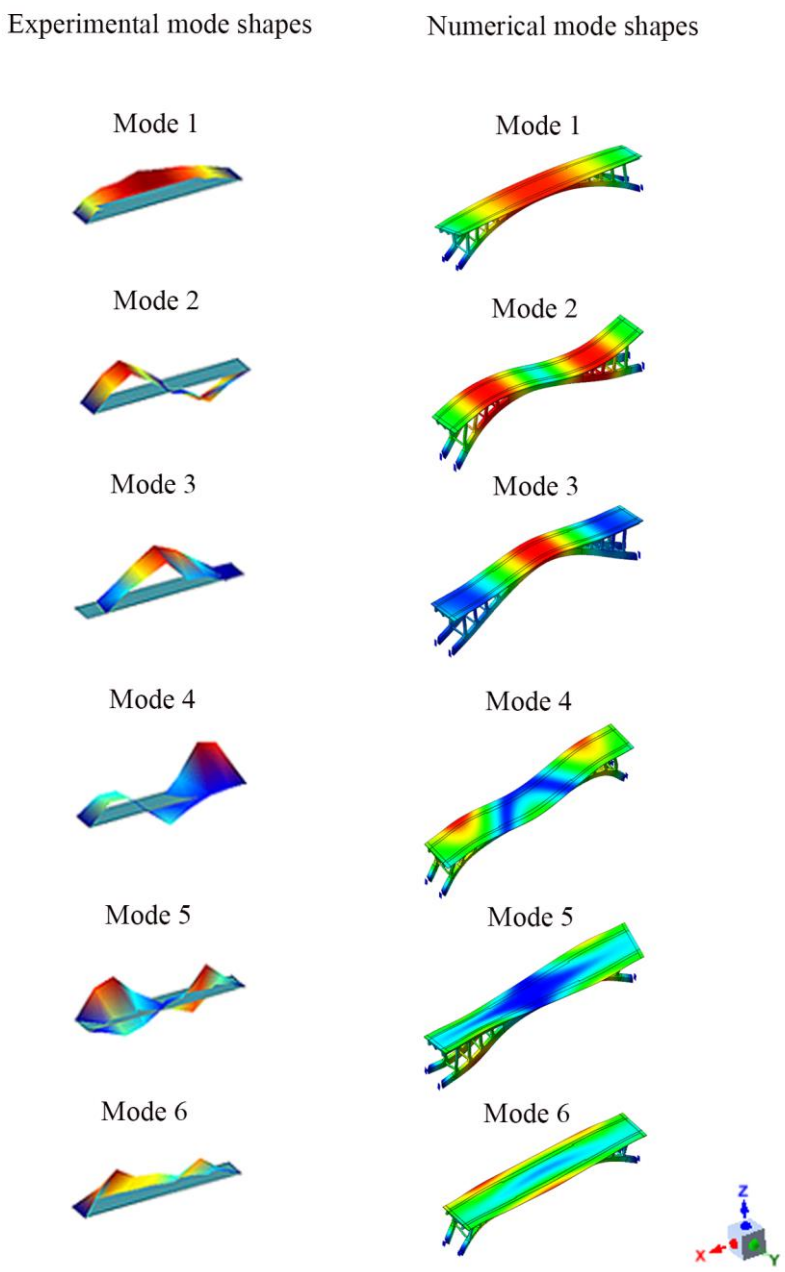

Figure 22: Graphical comparison between experimental and numerical modal shapes obtained in the second calibration stage.

5 Safety analysis

Considering the last calibrated model as the most accurate numerical representation of the bridge, an evaluation of the Ultimate Limit State (ULS) following the Eurocode recommendations [34-37] was carried out. During this evaluation, the maximum flexural capacity of each structural component and the compression axial forces in the pillars were compared (resistance values) with

the moments and the compression axial forces obtained by the numerical simulation (action values). Regarding the numerical simulation and considering the current limitations of the bridge (maximum weight of 12.00 tons, maximum height of 3.50 m and 2.50 m of maximum width), a modification of the loads proposed in the Load Model 1 (LM-1) (Fig. 23) was considered [36], namely: i) gravity load; ii) LM-1 distributed load of 4.00 kN/m^2 ; and iii) LM-1 concentrated load of 187.50 kN/m^2 (area of the wheels of 0.16 m^2 according with LM-1 of Eurocode).

These loads were combined applying the Eurocode, where the safety factors for the most unfavourable case were considered (1.2 for gravity load and 1.5 for distributed load and concentrated load), obtaining the flexural moments of all structural elements and the compression axial force in the pillars (Fig. 24).

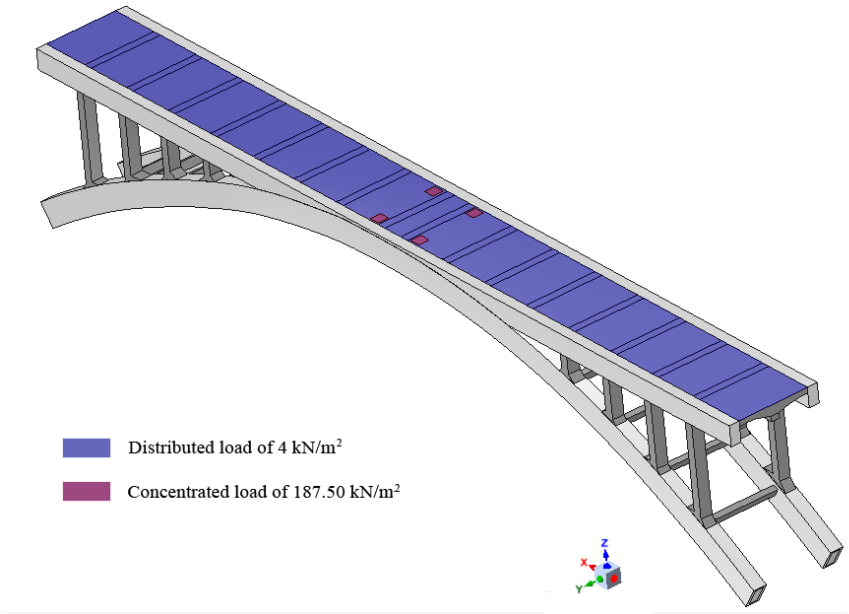

Figure 23: Considered loads according with LM-1 of Eurocode

PUBLISHED VERSION (DOI): 10.1016/j.conbuildmat.2017.10.084

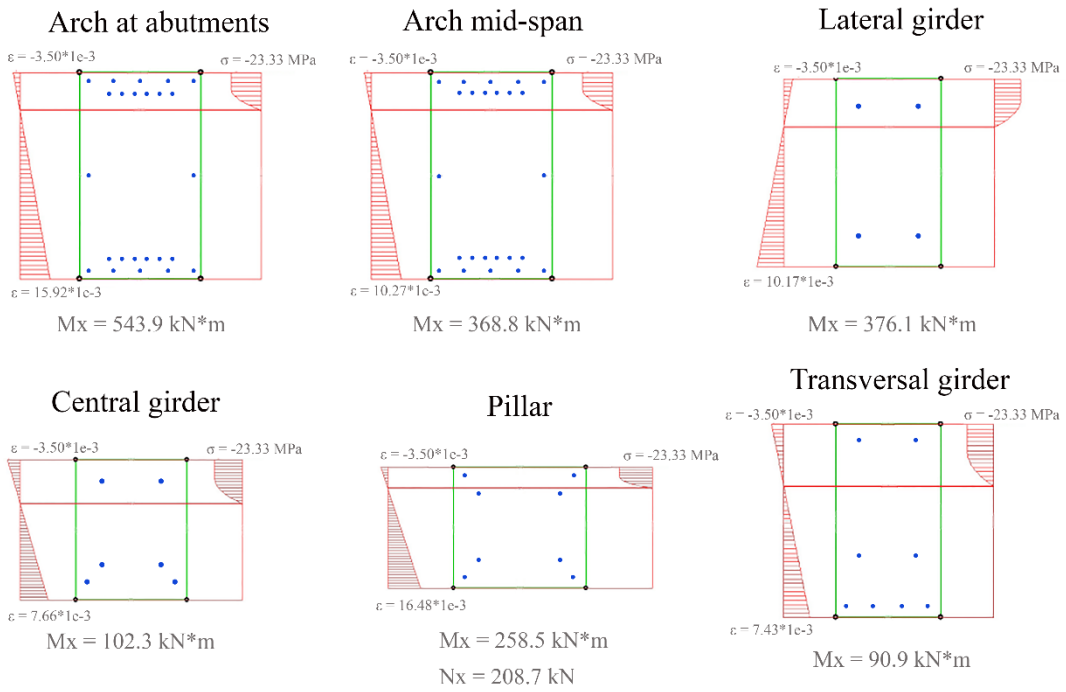

Figure 24: Maximum flexural capacity of structural members and maximum compression axial force in the pillars. Results obtained by CSA analysis [38].

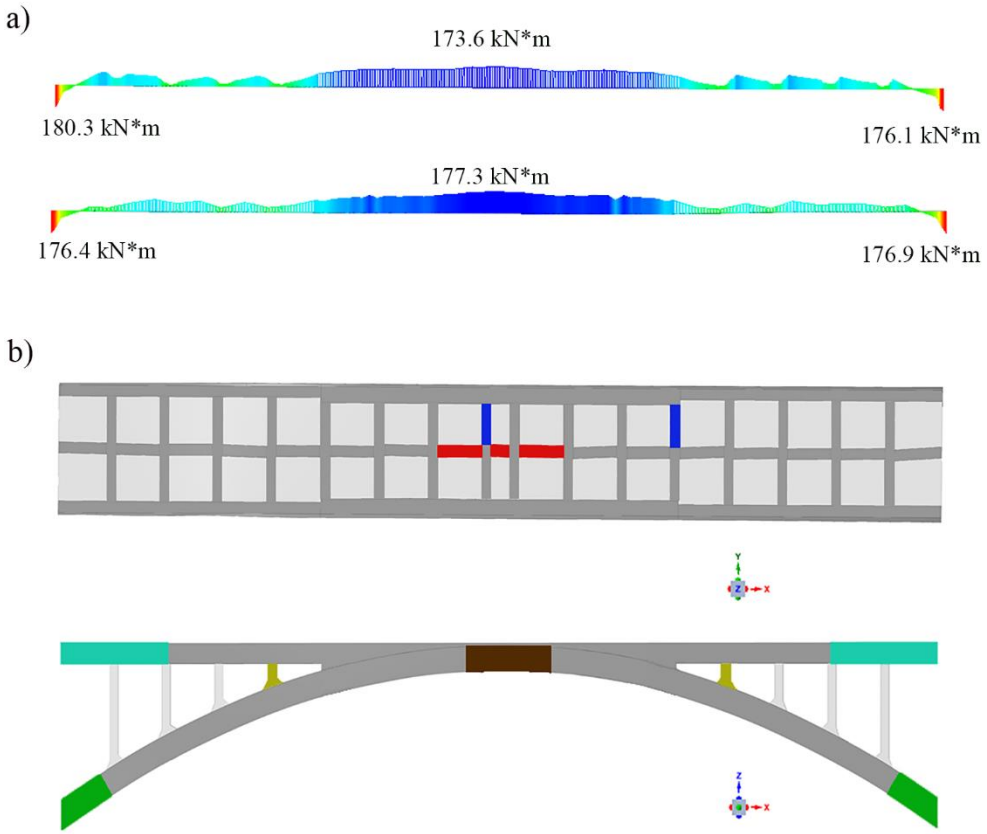

Figure 25: Results obtained during the safety evaluation: a) graphical representation of the flexural moments (arch girders) obtained though the FEM; and b) structural components evaluated.

Table 12: Results obtained during the safety evaluation.

Structural elements	Action values	Resistance values
$Mx_{Arch\_abutments}$	180.3 kN.m	543.9 kN.m
$Mx_{Arch\_mid\text{-}span}$	177.3 kN.m	368.8 kN.m
$Mx\_{Lateral\ girder}$	42.3 kN.m	376.1 kN.m
$Mx\_{Central\ girder}$	14.9 kN.m	102.3 kN.m
$Mx\_{\ Pillar}$	58.1 kN.m	258.5 kN.m
N_{Pillar}	71.5 kN	208.7 kN
$Mx\_{\ Transversal\ girder}$	40.6 kN.m	258.5 kN.m

Results obtained from the safety evaluation show that the most critical structural elements are the arch girders with a safety factor of 2.1 in the mid-span (Table 12) (Fig. 25), verifying the ULS.

6 Conclusions

This paper proposes a multidisciplinary approach focused on the evaluation of the current safety conditions of historic bridges erected in reinforcement concrete. The method combines terrestrial laser scanning, ambient vibration approaches and laboratory tests (e.g. scanning electron microscope or compression tests) with the aim of characterizing its geometry, dynamic response or materials used, and also to create accurate as-built numerical models and validate them.

To corroborate the robustness of the proposed method an early reinforcement concrete bridge was chosen as study case: the Bôco Bridge in the north of Portugal. However, the complexity of the numerical simulation led to a great computational effort, being necessary not only to perform an equivalent homogeneous numerical model, but also a cost-efficient calibration strategy to update the numerical simulation. To this end, firstly the second-order response surface of the cost function and its minimum was calculated through the combination of the Douglas-Reid and the genetic algorithm. This minimum was refined with the use of several mathematical strategies: the

non-linear least squares method, the gradient-based Gauss-Newton approach and the trust-reflective algorithm.

Thus, the proposed method obtained an accurate numerical simulation of the current conditions of the Bôco bridge, reducing the relative error in frequencies from an initial value of 32.46 % to 1.22 % and increasing the average MAC value from 0.87 to 0.91. This numerical model was used to estimate the current safety conditions of the bridge, comparing the maximum capacity of each structural element with the results obtained from the numerical evaluation. These results shown a bridge with enough capacity to bear the current solicitations (on which the most critical structural part was the arch girder in mid-span with an estimated safety factor of 2.1)

Futures works will be focused on the application of additional NDT tests such as sonic and ultrasonic or rebar detector tests with the aim of improving the knowledge about the materials used in the Bôco Bridge. Concerning the numerical model, it will be validated not only through the discrepancies between frequencies and modal shapes but also through different transient analysis with traffic actions. Additionally, several radiometric classifications (by means of pixel-based approaches), based on the data captured by the TLS system, will be carried out to complete the damage diagnosis of the bridge.

Acknowledgments

This work was financed by FEDER funds through the Competitiveness Factors Operational Programme - COMPETE and by national funds through FCT – Foundation for Science and Technology within the scope of the project POCI-01-0145-FEDER-007633. This research has been also partially supported by CHT2 – Cultural Heritage through Time – funded by JPI CH Joint Call and supported by the Ministerio de Economia y Competitividad, Ref. PCIN-2015-071.

References

[1] H. González-Jorge, D. Gonzalez-Aguilera, P. Rodriguez-Gonzalvez, P. Arias, Monitoring biological crusts in civil engineering structures using intensity data from terrestrial laser scanners, Construction and Building Materials 31 (2012) 119-128.

[2] F. Leonhardt, Bridges, 1984.

[3] A. Hellebois, A. Launoy, C. Pierre, M. De Lanève, B. Espion, 100-year-old Hennebique concrete, from composition to performance, Construction and Building Materials 44 (2013) 149-160.

[4] J.-L. Bosc, J.-M. Chauveau, J. Clément, J. Degenne, B. Marrey, M. Paulin, Joseph Monier et la naissance du ciment armé, Ed. du Linteau2001.

[5] M.L. Gambhir, Concrete Technology: Theory and Practice, Tata McGraw-Hill Education2013.

[6] F.P. Glasser, J. Marchand, E. Samson, Durability of concrete—degradation phenomena involving detrimental chemical reactions, Cement and Concrete Research 38(2) (2008) 226-246.

[7] J. Sena-Cruz, J.C. Araújo, F. Castro, M. Jorge, Assessment of the bôco historical RC bridge, SAHC2012–Structural Analysis of Historical Constructions (2012) 2214-2221.

[8] C. Costa, D. Ribeiro, P. Jorge, R. Silva, A. Arêde, R. Calçada, Calibration of the numerical model of a stone masonry railway bridge based on experimentally identified modal parameters, Engineering Structures 123 (2016) 354-371.

[9] J. Sena-Cruz, R.M. Ferreira, L.F. Ramos, F. Fernandes, T. Miranda, F. Castro, Luiz Bandeira Bridge: Assessment of a Historical Reinforced Concrete (RC) Bridge, International Journal of Architectural Heritage 7(6) (2013) 628-652.

[10] T. Zordan, B. Briseghella, T. Liu, Finite element model updating of a tied-arch bridge using Douglas-Reid method and Rosenbrock optimization algorithm, Journal of Traffic and Transportation Engineering (English Edition) 1(4) (2014) 280-292.

[11] D. Ribeiro, R. Calçada, R. Delgado, M. Brehm, V. Zabel, Finite element model updating of a bowstring-arch railway bridge based on experimental modal parameters, Engineering Structures 40 (2012) 413-435.

[12] T. Türker, A. Bayraktar, Structural safety assessment of bowstring type RC arch bridges using ambient vibration testing and finite element model calibration, Measurement 58 (2014) 33-45.

[13] L.J. Sánchez-Aparicio, L.F. Ramos, J. Sena-Cruz, J.O. Barros, B. Riveiro, Experimental and numerical approaches for structural assessment in new footbridge designs (SFRSCC–GFPR hybrid structure), Composite Structures 134 (2015) 95-105.

[14] H. Yoon, H. Song, K. Park, A phase-shift laser scanner based on a time-counting method for high linearity performance, Review of Scientific Instruments 82(7) (2011) 075108.

[15] A. Bienert, H.-G. Maas, Methods for the automatic geometric registration of terrestrial laser scanner point clouds in forest stands, International archives of the photogrammetry, remote sensing and spatial information sciences 38(part 3) (2009) W8.

[16] V.-S. Nguyen, A. Bac, M. Daniel, Simplification of 3D point clouds sampled from elevation surfaces, (2013).

[17] M. Herrero-Huerta, D. González-Aguilera, P. Rodriguez-Gonzalvez, D. Hernández-López, Vineyard yield estimation by automatic 3D bunch modelling in field conditions, Computers and electronics in agriculture 110 (2015) 17-26.

[18] J. Hoschek, W. Dankwort, Reverse engineering, Springer1996.

[19] R. Brincker, L. Zhang, P. Andersen, Modal identification from ambient responses using frequency domain decomposition, Proc. of the 18*'International Modal Analysis Conference (IMAC), San Antonio, Texas, 2000.

[20] C.E. de Normalisation, EN 1992–1–1 Eurocode 2: Design of Concrete Structures, Part I-1: Generai Rules and Rules for Buildings. CEN, Brussels (2004).

[21] N. Chouw, A. Pipinato, Dynamics of bridge structures, Innovative Bridge Design Handbook (2016) 127-153.

[22] T. Diana, DIANA-finite element analysis, The Netherlands (2005).

[23] A.K. Chopra, Dynamics of Structures, vol. 3, Prentice Hall, New Jersey, 1995.

[24] A. Kasahara, S. Matsuno, Estimation of apparent elastic modulus of concrete block layer, Proceedings of 3rd International Conference on Concrete Block Paving, 1988, pp. 142-147.

[25] R.J. Allemang, The modal assurance criterion–twenty years of use and abuse, Sound and vibration 37(8) (2003) 14-23.

[26] E. Simoen, G. De Roeck, G. Lombaert, Dealing with uncertainty in model updating for damage assessment: A review, Mechanical Systems and Signal Processing 56 (2015) 123-149.

[27] L. Myers, M.J. Sirois, Spearman correlation coefficients, differences between, Wiley StatsRef: Statistics Reference Online (2006).

[28] M.D. McKay, R.J. Beckman, W.J. Conover, Comparison of three methods for selecting values of input variables in the analysis of output from a computer code, Technometrics 21(2) (1979) 239-245.

[29] B.M. Douglas, W.H. Reid, Dynamic tests and system identification of bridges, Journal of the Structural Division 108(ST10) (1982).

[30] D.E. Goldberg, Genetic algorithms, Pearson Education India2006.

[31] L.J. Sánchez-Aparicio, A. Villarino, J. García-Gago, D. González-Aguilera, Photogrammetric, Geometrical, and Numerical Strategies to Evaluate Initial and Current Conditions in Historical Constructions: A Test Case in the Church of San Lorenzo (Zamora, Spain), Remote Sensing 8(1) (2016) 60.

[32] X. Chen, P. Omenzetter, S. Beskhyroun, Calibration of the Finite Element Model of a Twelve-Span Prestressed Concrete Bridge Using Ambient Vibration Data, EWSHM-7th European Workshop on Structural Health Monitoring, 2014.

[33] D.-S. Jung, C.-Y. Kim, Finite element model updating on small-scale bridge model using the hybrid genetic algorithm, Structure and Infrastructure engineering 9(5) (2013) 481-495.

[34] B.S. Institution, Eurocode 0 - Basis of structural design, BSI2004.

[35] E. STN, Eurocode 1: Actions on structures, Part 1-1: General actions, Densities, self-weight, imposed loads for buildings, Slovak Office of Standards, Metrology and Testing (2007).

[36] C. Eurocode, 1: Actions on structures, Part 2: Traffic loads on bridges, Brussels: European Standard EN 2 (1991) 2003.

[37] C.R. Hendy, D.A. Smith, Designers' Guide to EN 1992-2: Eurocode 2: Design of Concrete Structures. Concrete bridges, Thomas Telford2007.

[38] H. Miranda, Á.F. Azevedo, J. Sena-Cruz, Cálculo orgânico de secções quaisquer em flexão desviada segundo o Eurocódigo 2, Encontro Nacional Betão Estrutural 2008: actas (2008) 1-10.